Journal of Coastal Research	16	3	790–799	West Palm Beach, Florida	Summer 2000

Evaluations on Coastal Topographical Changes at Hualien Coast, Taiwan

Tai-Wen Hsu†, Shan-Hwei Ou†, and Shiaw-Yih Tzang‡

†Department of Hydraulics and Ocean Engineering
National Cheng Kung University
Tainan 701, Taiwan

‡Department of River and Harbor Engineering
National Taiwan Ocean University
Keelung 202, Taiwan

ABSTRACT

HSU, T.W.; OU, S.H., and TZANG, S.Y., 2000. Evaluations on coastal topographical changes at Hualien Coast, Taiwan. *Journal of Coastal Research,* 16(3), 790–799. West Palm Beach (Florida), ISSN 0749-0208.

Coastal topographical changes at Hualien Coast, downdrift of Port of Hualien, Taiwan, after the construction of an extended breakwater are closely evaluated based on the results from continuous field survey data, a statistical 2-D empirical eigenfunction model, and a numerical hydrodynamic model for nearshore current fields. Firstly, the analysis from field survey data verifies the significant impacts on shoreline changes due to the installation of an extended breakwater. The 2-D empirical eigenfunction model is then applied to forecast beach profile changes at the coastal areas assuming no breakwater installation. Comparisons with surveyed beach profiles successfully illustrate that the breakwater installation is responsible for giving rise to accreting northern beaches while eroding southern beaches. The numerical result further points out that the extended breakwater induces an extra clockwise circulation cell in harbor's lee marine area and it transports sediment towards the harbor in shallower water. Altogether, clear identifications on the effects of the breakwater installation suggest that detailed and reliable evaluations on the coastal topographical changes can be achieved through adoption of the present schemes.

ADDITIONAL INDEX WORDS: *Coastal topographical changes, empirical eigenfunction model, wave-induced nearshore circulation, beach erosion.*

INTRODUCTION

Hualien Coast, facing the Pacific Ocean, is located in the middle east coast of Taiwan. It is bounded by the Meilum River in the north, the Hualien River in the south and is nearby the west out-skirt breakwater of Port of Hualien as shown in Figure 1. Figure 2 illustrates that the studied breakwater began construction from 1987 to be extended from the old eastern out-skirt breakwater to deeper depths. It was primarily installed to protect Port of Hualien, the most important harbor in the eastern coast of Taiwan, from storm wave attacks during summer periods.

Coastal structures on sandy beaches are prone to interfering with existing sediment transports and usually result in coastal topographical changes. According to historical records and local interviews at Hualien Coast the beach widths above mean water level were about 100 to 200 meters in front of the old seawalls before 1954 and were slowly retreating since then. But after the completion of the extended breakwater in 1989, the Hualien Coast has been reported to have experienced significant coastal topographical changes in the following few years. As a result, the southern shoreline is retreating rapidly approaching the new seawalls while increasing sediments have been accumulated on the northern beach, especially near the outlet of Meilum River (WATER CONSERVANCY BUREAU, 1989). These outcomes seem to suggest that the latest extended breakwater is most responsible for the changes of coastal processes at Hualien Coast. Therefore, it is the primary object of this paper to adopt different schemes to closely evaluate the coastal topographical changes for clarifying the causes so as to take most suitable countermeasures to stabilize the Hualien Coast in the future.

Two technical schemes together with periodical field hydrographic survey data are utilized to carry out the work. Field surveying was performed bi-monthly since 1980. The beach profile changes above mean water level were most emphasized. The survey area has a total alongshore length of about 4 km with 16 beach profiles each with a distance of 250 m apart for studying beach profile evolution as specified in Figure 1. Routine survey work was discontinued from July 1987 to 1989 during the periods of breakwater constructions. In the later analyses, bi-monthly survey beach profile data from June, 1984 to June, 1987 are examined to verify the beach changes before breakwater installations. The data resumed in 1989 are studied to illustrate coastal topographical changes after breakwater installation and compared with predictions by the statistical model. In the end, detailed calculations of the wave-induced nearshore hydrodynamics by a numerical model have further identified the causes of coastal topographical changes.

SHORELINE CHANGES

At Hualien Coast the slope of sea bottom is comparatively steep. Past geological records have shown that large quanti-

98045 received 11 March 1998; accepted in revision 27 September 1999.

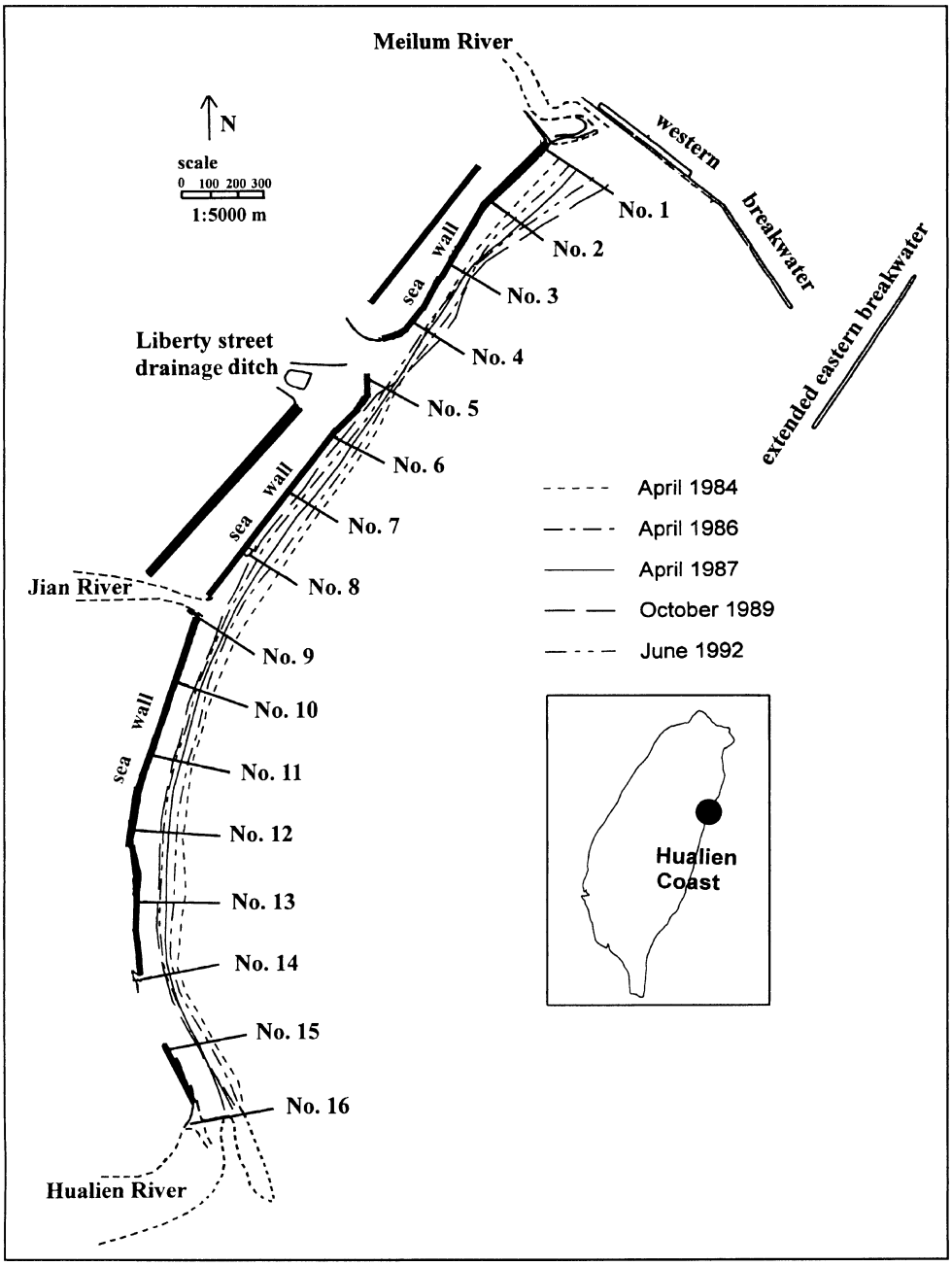

Figure 1. Location, measured beach profiles and shoreline changes of Hualien Coast, Taiwan.

ties of sediments were discharged from several nearby rivers. Most of the sediments are lost to submarine canyons without returning to the shore. Still, some of the sediments mainly supplied from Hualien River and Meilum River are transported in the longshore direction to build beach zones along the coast. Because of the small amounts of sediments from Jian River and influent flow from Liberty Street drainage ditch (see Figure 1), their impact on coastal processes is assumed to be negligible. In recent years, sediments supplied to the beach have been further reduced due to many projects of flood control at the upstream of Hualien River, resulting in beach erosion from profiles No. 9 to No. 16 due to the shortage of beach material supplied to the shore.

According to the Water Conservancy Bureau (1989), the survey data of beach profiles have clearly demonstrated that shorelines slightly fluctuated back and forth along this coast before 1987, but the changes increased after 1987. In Figure 1, it can be immediately noticed that from 1984 to 1992, the shorelines between profiles No. 1 and No. 4 moved seawards while those between No. 5 and No. 16 moved landwards. The

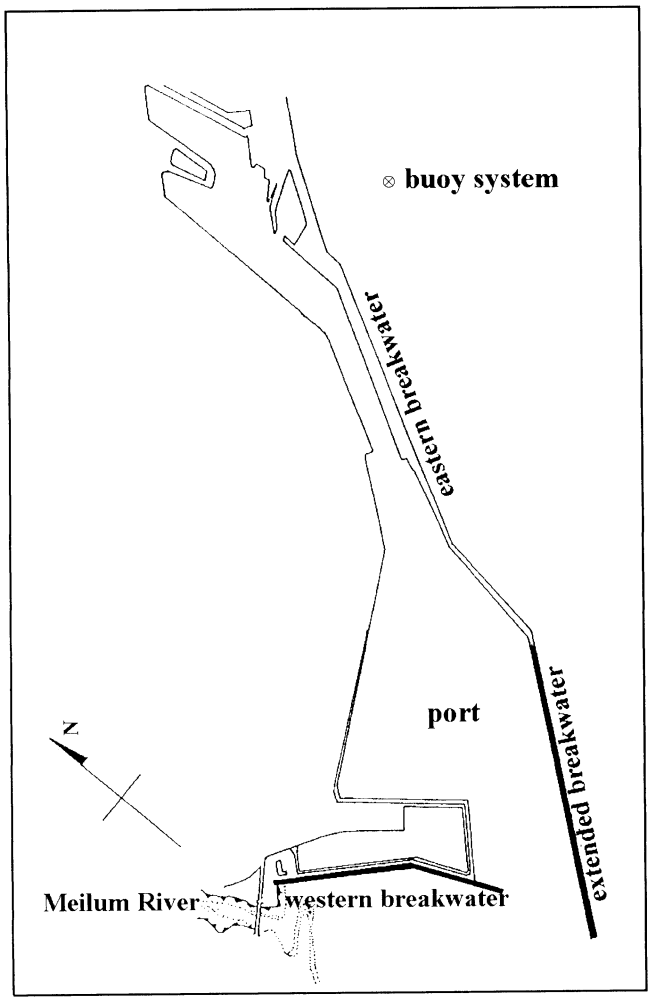

Figure 2. Layout of Hualien Harbor and location of wave buoy system.

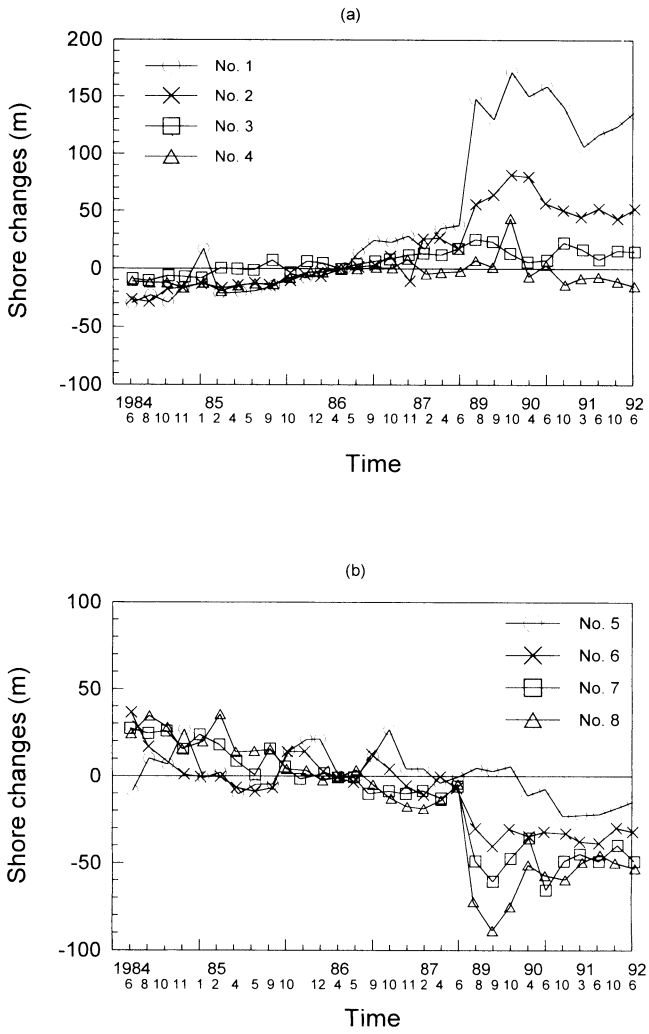

Figure 3. A comparison of temporal shoreline changes at different beach profiles. (a): No. 1 ~ No. 4; (b): No. 5 ~ No. 8.

beach is nearly in dynamic equilibrium after installations of four units of detached breakwaters along profiles No. 5 to No. 8 in 1991.

Shoreline changes before and after the completion of the extended breakwater are further illustrated by the detailed shoreline evolution during the same periods at profiles close to the harbor. By taking the data in April, 1986 as the datum, Figure 3 shows that shoreline changes at Hualien Coast from No. 1 to No. 8 had experienced more significant changes after 1986 than before. Once again, the survey data clearly demonstrate that shorelines advanced in the coastal regions between profiles No. 1 to No. 4 and retreated in the downstream profiles No. 5 to No. 8. As a result, these outcomes indicate that the installation of the extended breakwater have played an important role in changing beach processes at Hualien Coast. Next, we shall further verify the beach profile changes due to engineering constructions rather than to natural evolution by applying two technical schemes to evaluate the effects of the extended breakwater on Hualien Coast and to identify the associated mechanism.

PRINCIPLE OF TECHNICAL SCHEMES

2-D Empirical Eigenfunction Model

The adopted technical schemes mainly consist of methodologies in terms of statistical and numerical calculations, respectively. The empirical eigenfunction model (HSU *et al.*, 1994) which was simplified from a previous version with 2-D empirical eigenfunctions (HSU *et al.*, 1986) is performed on the basis of field survey beach profile data. Similar statistical schemes have been applied to the examination of beach profile changes by different researchers (*e.g.* WINANT *et al.*, 1975; AUBREY, 1978; PRUSZAK, 1993; *etc.*). It is also found to be efficient and advisable for predicting the beach variations around coastal structures (UDA and HASHIMOTO, 1982; HSU *et al.*, 1994).

According to HSU *et al.* (1994), the spatial and temporal beach bed elevations h(x, y, t) can be expressed as the sum of a mean and the fluctuations:

$$h(x, y, t) = \bar{h}(x, y) + \sum_k a_k e_k(x)\, e_k(y)\, c_k(t) \quad (1)$$

where $\bar{h}(x, y)$ represents the time averaged beach profile, x is the offshore distance, y the longshore distance, a_k the orthogonal factors, $e_k(x)$ the cross-shore eigenfunctions, $e_k(y)$ the longshore eigenfunctions, $c_k(t)$ the temporal eigenfunctions, and k the variation modes. As can be seen from Equation (1), the eigenfunctions are all orthogonal and shall be obtained from input data sets. Since beach profile changes are mainly concerned with temporal variations, the present model can predict next time step beach profile changes based on known parameters. Assuming the beach profile changes follow the Markov process (SONU and JAMES, 1973) with one forcing parameter, the subsequent time step eigenfunctions $c_k(t + 1)$ are to be derived by allowing spatial eigenfunctions $e_k(x)$ and $e_k(y)$ to remain unchanged. As a result, the simple linear equations for $c_k(t + 1)$ at each mode k can be written in a matrix form as

$$\begin{bmatrix} c_1(t+1) \\ c_2(t+1) \\ \vdots \\ c_n(t+1) \end{bmatrix} = \begin{bmatrix} a_{11} & a_{12} & \cdots & a_{1n} & a_{1(n+1)} \\ a_{21} & a_{22} & \cdots & a_{2n} & a_{2(n+1)} \\ \vdots & & & & \vdots \\ a_{n1} & a_{n2} & \cdots & a_{nn} & a_{n(n+1)} \end{bmatrix} \begin{bmatrix} c_1(t) \\ c_2(t) \\ \vdots \\ c_n(t) \\ F(t+1) \end{bmatrix} \quad (2)$$

where $a_{11}, \ldots, a_{n(n+1)}$ are constant coefficients, and $F(t + 1)$ is the dimensionless forcing parameter within the time intervals of t and t + 1. The forcing parameter ξ_0 as proposed by HSU *et al.* (1994) was found to be appropriate in describing coastal processes and beach profile changes. It is called the modified Iribarren number which takes account of incident wave conditions (wave height at deep water H_0, wave length at deep water L_0, and wave incident angle θ) as well as beachface slope $\tan \beta$, and is defined as

$$\xi_0 = \frac{\tan \beta}{\sqrt{H_0/L_0}} \cos \theta \quad (3)$$

In a general matrix notation, Equation (2) can be rewritten as

$$P = AD \quad (4)$$

where P is a m × N matrix with m quantities to be predicted, D is a n × N matrix with n data parameters, and A is an m × n coefficient matrix. For total N observations, the optimal form of the coefficient matrix A is determined by applying the linear regression method:

$$A = C_{PD}C_{DD}^{-1} = (PD^T)(DD^T)^{-1} \quad (5)$$

where C_{PD} denotes the covariance matrix between the predictand and field data, C_{DD} is the auto-covariance matrix of the data, and the note T represents the transpose of a matrix. The forecast ability is described by the mean-square forecast error index S_F defined as

$$S_F = \frac{E[h(x, y, t) - \hat{h}(x, y, t)][h(x, y, t) - \hat{h}(x, y, t)]^T}{E[h(x, y, t)h(x, y, t)^T]} \quad (6)$$

where $\hat{h}(x, y, t)$ is the estimated bed elevation, E denotes the expectation of the variables. As is known, predictions usually become more reliable as the value of S_F is small.

Nearshore Hydrodynamic Models

Waves

The numerical scheme focuses on the simulations of the wave field and wave-induced nearshore currents, which are critical to the sediment transport in the nearby coastal areas. In the present scheme, the wave fields are based on the transient mild-slope equations given by BOOIJ (1981) as

$$\frac{\partial^2 \Phi}{\partial t^2} - \nabla \cdot (CC_g \nabla \Phi) + (\omega^2 - k^2 CC_g)\Phi = 0 \quad (7)$$

where C is the wave celerity, C_g the group wave velocity, Φ the velocity potential, k the wave number, ω the wave frequency, t the time, $\nabla = (\partial/\partial x, \partial/\partial y)$ the horizontal gradient operator, x the offshore distance measured from the original shoreline, and y the alongshore distance. This equation was modified from the mild-slope equation derived by BERKHOFF (1972) and is capable of simulating combined effects of wave refraction, diffraction and reflection.

The current status of BOOIJ's mild-slope equation is unable to simulate wave breaking and energy dissipation in the surf zone. It is essential to develop a model describing wave transformation in the surf zone to provide reasonable information of wave-induced nearshore current. To incorporate wave energy dissipation due to wave breaking into mild-slope equation, an empirical energy dissipation presented by ISOBE (1987) is added to Equation (7) as follows

$$\frac{\partial \Phi}{\partial t^2} - \nabla \cdot (CC_g \nabla \Phi) + [\omega^2 - k^2 CC_g(1 + if_d)]\Phi = 0 \quad (8)$$

where $i = \sqrt{-1}$ is the imaginary number, f_d is the dissipation coefficient defined as

$$f_d = \frac{5}{2} \tan \beta \sqrt{\frac{1}{k_0 h}\left(\frac{\gamma - \gamma_r}{\gamma_s - \gamma_r}\right)} \quad (9)$$

where k_0 is the wave number at deep water, γ denotes a ratio value defined as

$$\gamma = a/h \quad (10)$$

where a is the amplitude of water surface displacement, h is the mean water depth. The parameters γ_r and γ_s are given, respectively, as

$$\gamma_r = 0.135 \quad (11)$$

$$\gamma_s = 0.4 \times (0.57 + 5.3 \tan \beta) \quad (12)$$

According to ISOBE (1987), a breaking index γ_b is used as the breaking criterion defined by

$$\gamma_b = 0.53 - 0.3 \exp(-3\sqrt{h_b/L_0}) + 5(\tan \beta)^{2/3} \exp[-45(\sqrt{h_b/L_0} - 0.1)^2] \quad (13)$$

where h_b is the breaking water depth. The above breaking wave model has been shown to be applicable for simulating wave transformation in the surf zone (HSU and WEN, 1998).

The partial radiation boundary conditions are specified by

$$\frac{\partial \Phi}{\partial x} \mp ik \cos\theta \Phi = 0; \quad \text{on } \partial B_x, \text{ or } \partial B_x \tag{14a}$$

$$\frac{\partial \Phi}{\partial y} \mp ik \sin\theta \Phi = 0; \quad \text{on } \partial B_y, \text{ or } \partial B_y \tag{14b}$$

where θ is the approaching wave angle, ∂B_x (or ∂B_y) is the boundary perpendicular to the x (or y) axis. Equation (8) subjected to radiation conditions is solved numerically by the Alternating Direction Implication (ADI) method. Details are referred to HSU and WEN (1998).

Nearshore Currents

The wave-induced nearshore currents are calculated based on the computed wave field. The two-dimensional depth-averaged governing equations for a mean flow are written as (HORIKAWA, 1988)

$$\frac{\partial \bar{\zeta}}{\partial t} + \frac{\partial (UD)}{\partial x} + \frac{\partial (VD)}{\partial y} = 0 \tag{15}$$

$$\frac{\partial U}{\partial t} + U\frac{\partial U}{\partial x} + V\frac{\partial U}{\partial y} + F_x - M_x + R_x + g\frac{\partial \bar{\zeta}}{\partial x} = 0 \tag{16}$$

$$\frac{\partial V}{\partial t} + U\frac{\partial V}{\partial x} + V\frac{\partial V}{\partial y} + F_y - M_y + R_y + g\frac{\partial \bar{\zeta}}{\partial y} = 0 \tag{17}$$

where D is the total water depth, *i.e.* $D = h + \bar{\zeta}$, (U, V) are the x and y components of the mean current, $\bar{\zeta}$ is the mean water surface elevation, F_x and F_y are bottom friction terms in the x and y directions and are given by (NISHIMURA, 1982)

$$F_x = \frac{C_f}{D}\left\{\left(W + \frac{\omega_b^2}{W}\cos^2\alpha\right)U + \frac{\omega_b^2}{W}\cos\alpha \sin\alpha V\right\} \tag{18}$$

$$F_y = \frac{C_f}{D}\left\{\left(W + \frac{\omega_b^2}{W}\sin^2\alpha\right)V + \frac{\omega_b^2}{W}\cos\alpha \sin\alpha U\right\} \tag{19}$$

$$W = \{\sqrt{U^2 + V^2 + \omega_b^2 + 2(U\cos\alpha + V\sin\alpha)\omega_b} + \sqrt{U^2 + V^2 + \omega_b^2 - 2(U\cos\alpha + V\sin\alpha)\omega_b}\}/2 \tag{20}$$

where C_f is the friction coefficient, α is the breaking wave angle, $\omega = \pi H/T \sinh kh$, H is the local wave height, and T is the wave period. M_x and M_y are lateral mixing terms written as

$$M_x = \frac{\partial}{\partial x}\left(\epsilon\frac{\partial U}{\partial x}\right) + \frac{\partial}{\partial y}\left(\epsilon\frac{\partial U}{\partial y}\right) \tag{21}$$

$$M_y = \frac{\partial}{\partial x}\left(\epsilon\frac{\partial V}{\partial x}\right) + \frac{\partial}{\partial y}\left(\epsilon\frac{\partial V}{\partial y}\right) \tag{22}$$

in which ϵ is the momentum change coefficient and is assumed in the form proposed by LONGUET-HIGGINS (1970) as

$$\epsilon = N\ell\sqrt{gD} \tag{23}$$

where N is a constant value smaller than 0.016, ℓ is a length characterized by $\ell = D/\tan\beta$. R_x and R_y are radiation stresses, and are given by

$$R_x = \frac{1}{\rho D}\left(\frac{\partial S_{xx}}{\partial x} + \frac{\partial S_{xy}}{\partial y}\right) \tag{24}$$

$$R_y = \frac{1}{\rho D}\left(\frac{\partial S_{yx}}{\partial x} + \frac{\partial S_{yy}}{\partial y}\right) \tag{25}$$

where ρ is the density of water, S_{xx}, S_{xy}, S_{yx} and S_{yy} denote the radiation stress components.

The complete equations are solved by the ADI method in which the staggered grid scheme is used for the numerical analysis. The offshore boundary is specified in such a way that the mean water surface level is not changed by any of the nearshore current within the model, that is

$$\bar{\zeta}(M, J) = 0; \quad \text{for all } J = 1, N$$

where M and N denotes the total grid points in the x and y directions, respectively.

The shoreline boundary condition is

$$U(1, J) = 0 \quad \text{and} \quad V(1, J) = 0; \quad \text{for all } J = 1, N$$

This equation states that there is no flow into or out of the beach. The lateral boundary conditions are for lateral open boundaries by specifying the derivatives of the current conditions, i.e.

$$\left.\begin{aligned} U(I, 1) &= U(I, 2) \quad \text{and} \quad V(I, 1) = V(I, 2) \\ U(I, N) &= U(I, N + 1) \quad \text{and} \quad V(I, N) = V(I, N + 1) \end{aligned}\right\}$$
$$\text{for all } I = 1, M$$

RESULTS AND DISCUSSIONS

Beach Profile Changes

For statistical analysis, there are a total of 19 time-varient beach profile data sets for 16 beach profiles measured every two months from June, 1984 to June, 1987. During July, 1987 to July, 1989, the extended breakwater was just under construction and no survey data were available for the analysis. The wave data observed at the offshore region of Hualien Harbor are used as a forcing parameter in the eigenfunction model. As shown in Figure 2, a wave buoy system was installed by CHANG and TZENG (1993) at a water depth of 30 m and the analog signals are digitized with a sampling rates of 2.56 Hz to achieve a good resolution of wave heights. The beach face-slope tan β is estimated on the basis of measured beach profiles at each time step. The modified Iribarren numbers are then computed by Equation (3) for every two months.

The error index S_F is first evaluated in order to examine the applicability of the 2-D empirical eigenfunction model as mentioned above. The first 16 time interval data sets are analyzed to derive statistical parameters for forecasting beach profiles in the time interval of 19th measured profile. The averaged value of S_F for all 16 beach profile is around 0.05 and this result confirms the forecast ability of the present model. Beach profiles along profiles No. 7 and 8 in 1987 are taken as the typical predicted examples to be compared with the surveyed beach profiles. Figure 4 shows good agreements at both profiles between predicted and measured results to a shallow water region about 140 meters offshore. In the figure, the initial beach profiles are also given to ensure that the differences in the predicted and measured profiles are considerably smaller than those of the initial and final measured profiles. These results suggest that this statistical model could be reasonably utilized to forecast beach profile changes after 1987 assuming no extended breakwater. Thus, comparisons of these predicted data with the measured data after

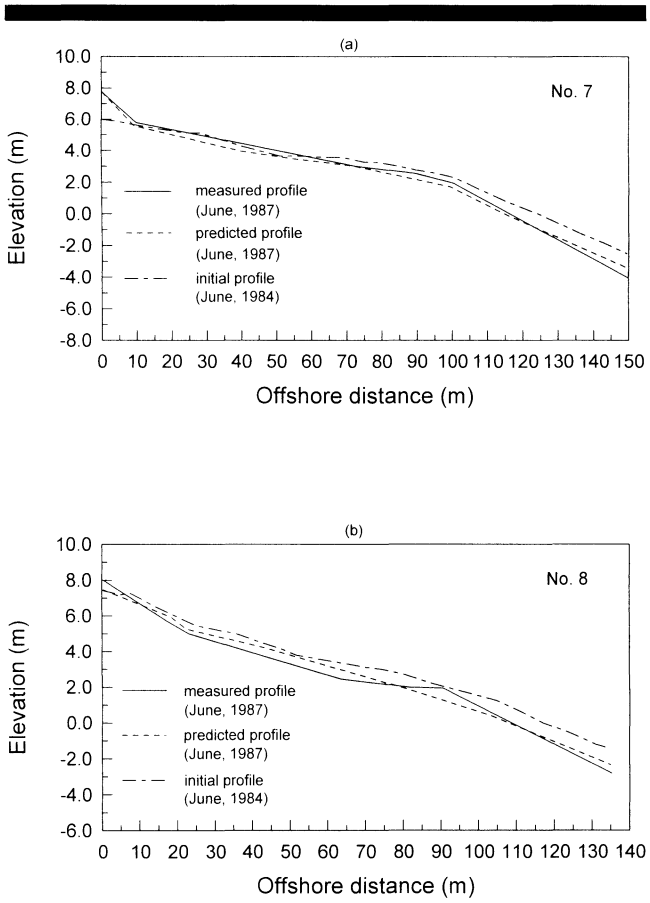

Figure 4. Verifications of the predictive eigenfunction model at beach profiles (a): No. 7 and (b): No. 8.

installing the extended breakwater could help to clarify the causes resulting in coastal topographical changes. To carry out this task, all the 19 time interval data sets of beach profiles before 1987 were used as the input to the statistical model for generating the corresponding eigenfunctions. These eigenfunctions are then used to forecast beach profile changes in June, 1989 when the extended breakwater had been completely installed.

Four beach profiles close to transition profile No. 4 (*i.e.* No. 1, No. 2, No. 7 and No. 8) are selected to demonstrate comparisons between the predicted (dashed lines) and measured profiles (solid lines) as shown in Figure 5. The initial profiles were also drawn in the figure for the comparison. All the four measured beach profiles are based on a coordinate system with the bench marks located at the fixed points on new seawalls. In general, the comparisons immediately display that beach profiles are greatly changed by the extended breakwater since the differences between predicted profiles assuming no extended breakwater and the measured profiles are remarkable. The differences become even more significant in the nearshore areas at profiles No. 1 and No. 2 due to beach accretion. The difference at profiles No. 7 and No. 8 are increasing in the offshore direction due to beach erosion. From Figures 5(a) and 5(b) (profiles No. 1 and No. 2), it is noted that considerably more beach accretion than the forecast beach profiles are found in this region resulting in steeper beach slopes. On the contrary, Figures 5(c) and 5(d) show that the installed extended breakwater causes the beach to be eroded at profiles No. 7 and No. 8 and the shorelines retreated for more than 50 m. Similar retreating tendencies based on comparisons of the forecast and measured beach profiles occurs along the other profiles but become less significant for those farther downstream. Clearly, the predicted beach profiles by the present statistical model has confirmed that the Hualien Coast is greatly affected by the breakwater installation but the underlying mechanism inducing such variations of coastal processes has not been clear yet. We shall attempt to identify the mechanism by applying numerical schemes to evaluate the wave and current fields in the nearshore water regions.

Waves and Nearshore Current Fields

For numerical calculations, typical incident waves for both monsoon and storm wave conditions are selected from previous reports (Ou *et al.*, 1992), as shown in Table 1, to evaluate their impacts on the coastal areas before and after the installation of the extended breakwater. Topographical information are based on the survey data and discretized for numerical calculations. Figures 6(a) and 6(b) show the calculated wave height distributions in the coastal zones due to monsoon wave conditions before and after the extended breakwater installation. By comparing both results, it is seen that waves are reduced in the coastal zones just downstream of the breakwater due to its extension. Clearly, the extended breakwater has imposed major sheltering effects on the Hualien Coast, while those due to pre-extended west breakwater is relatively minor since no noticeable coastal topographical changes has been found. Similar consequences of the sheltering effects by the extended breakwater can also be found for cases with storm wave conditions as shown in Figure 6(c). Figure 7 shows the calculated wave rays for the monsoon wave condition. In Figure 7(a), the effect of wave diffraction caused by the western breakwater is not significant except on the coastal areas from beach profiles No. 1 to No. 2. Figure 7(b) clearly shows that wave diffraction in the shadow zone of the eastern breakwater become remarkable in the region from beach profiles No. 1~No. 4. Wave energy spreads laterally on the sheltered side from the breakwater. From Figures 6 and 7, it is confirmed that the extended breakwater has a dominating influence on the nearshore hydrodynamics and, as a harbor protection facility, it effectively reduced the wave actions approaching the harbor entrance.

As has been discussed, wave spread in the lee side of the eastern breakwater is expected because of wave refraction and diffraction. Therefore, there is a directional spread of wave energy and there will be a portion of the wave energy that transports sediment in the lee of the breakwater extension. Without the presence of the extension, waves would occur from directions that could mobilize and transport sediment from the depositional area.

Based on the computed wave fields, we then calculated the wave-induced currents in the nearshore zones as shown in

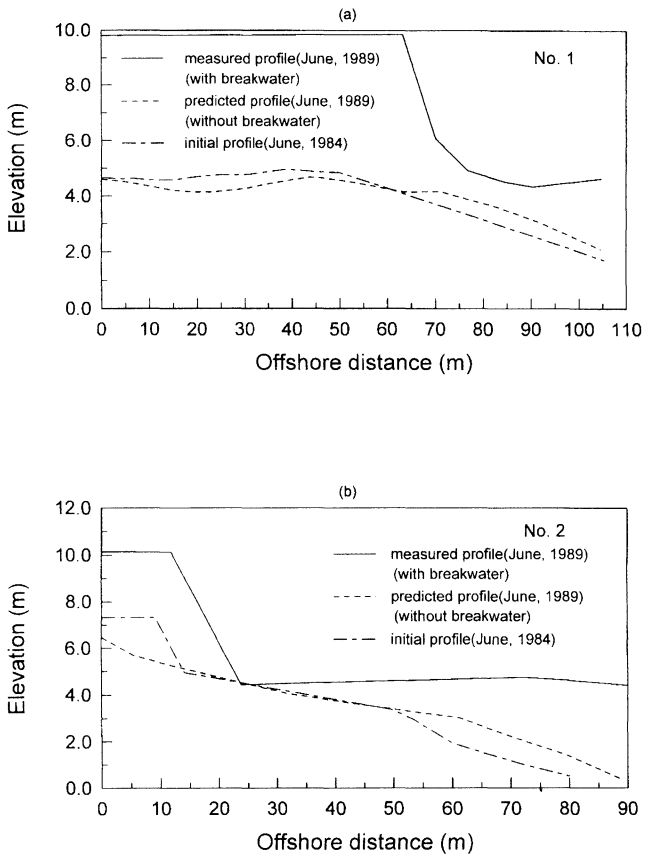

Figure 5. A comparison of beach profile changes before and after the extended breakwater installation; (a): profile No. 1; (b): profile No. 2; (c): profile No. 7; (d): profile No. 8.

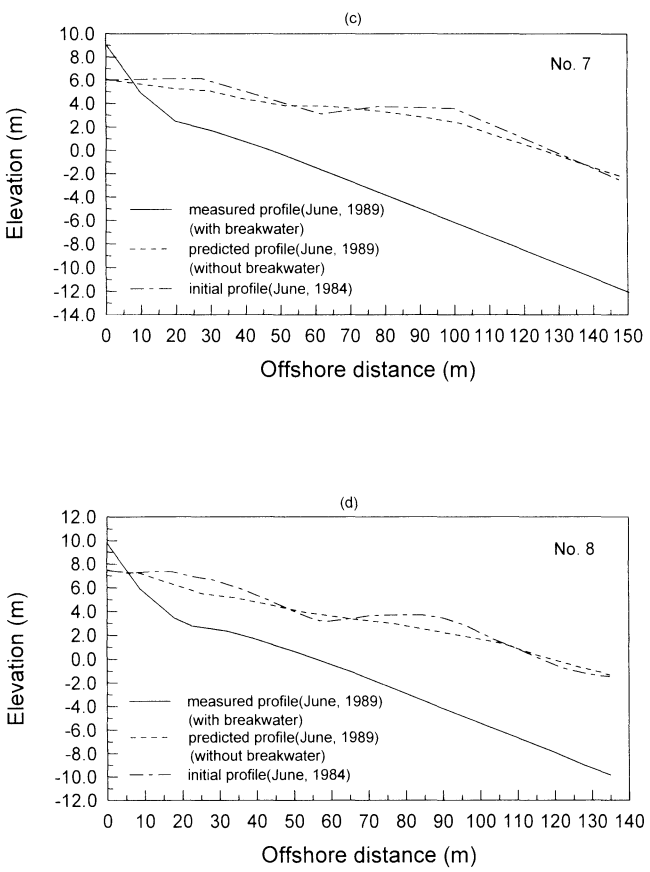

Figure 5. Continued.

Figure 8 before and after breakwater installation due to monsoon and storm waves, respectively. Figure 8(a) is the case without extended breakwater which displays that the monsoon waves induce small-scaled nearshore currents moving away from the Port of Hualien. Figure 8(b) evidently points out that the extended breakwater causes a slightly larger clockwise circulation in the coastal water between beach profiles No. 6 and No. 7. The same trends are found for storm waves-induced current fields, but the magnitudes are larger and the circulations become greater in coastal water closer to Hualien Harbor. The results in Figure 8(a) reveal that the dominant sediment transport is from north to south, which imply beach erosion in the northern beach before the construction of the breakwater. On the other hand, we notice from Figures 8(b) and 8(c) that there is a separation point between two circulation cells and a long term shortage of sediment supply from nearby rivers leads to the eroding southern beach after the completion of the breakwater. In Figures 8(b) and 8(c), the clockwise circulation moves towards the Harbor in the shallow water region while away from it in the deeper water region. As a result, coastal sediments, once initiated in the surf zone, are susceptible to the nearshore currents, especially those in the very nearshore region are carried towards the harbor. Additionally, sediment transport in this coastal water region is greatly increased during storm waves attacks several times a year since it is constantly subjected to actions of West Pacific Typhoons, especially during summer.

The extra circulation formed in the lee of the eastern breakwater extension can also be interpreted as the changes of breaking wave height and wave angle. The changed wave condition in the lee of breakwater extension leads to the differential wave set-up which occurs along the sheltered shoreline as a result of the redistribution of wave heights. This would drive a longshore current toward the north. Thus, by numerical calculations of the nearshore hydrodynamics, the shoreline changes and coastal topographical variations become clarified, meanwhile the causes of the beach accumulation at beach profiles No. 1 and No. 2 are also clearly iden-

Table 1. *Computational wave conditions.*

Waves	Wave Height (m)	Wave Period (sec)	Wave Angle (deg.)
Monsoon wave	4.0	8.0	ENE
Storm wave	10.8	14.8	E

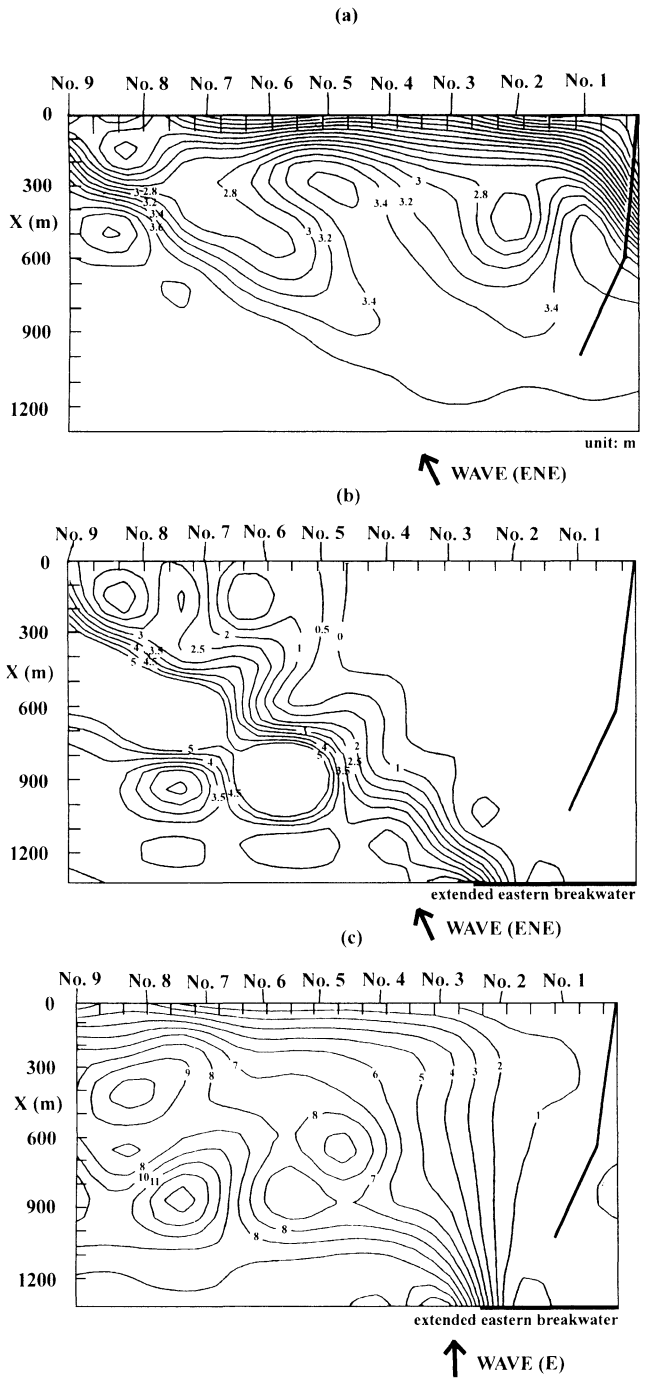

Figure 6. Wave heights at Hualien Coast before and after the extension of the eastern breakwater; (a): monsoon wave action without extended breakwater; (b): monsoon wave action with extended breakwater; (c): storm wave action with extended breakwater.

tified. The changes of nearshore hydrodynamics and wave-induced nearshore circulation cells due to the extended breakwater installation are most responsible for shoreline redistributions.

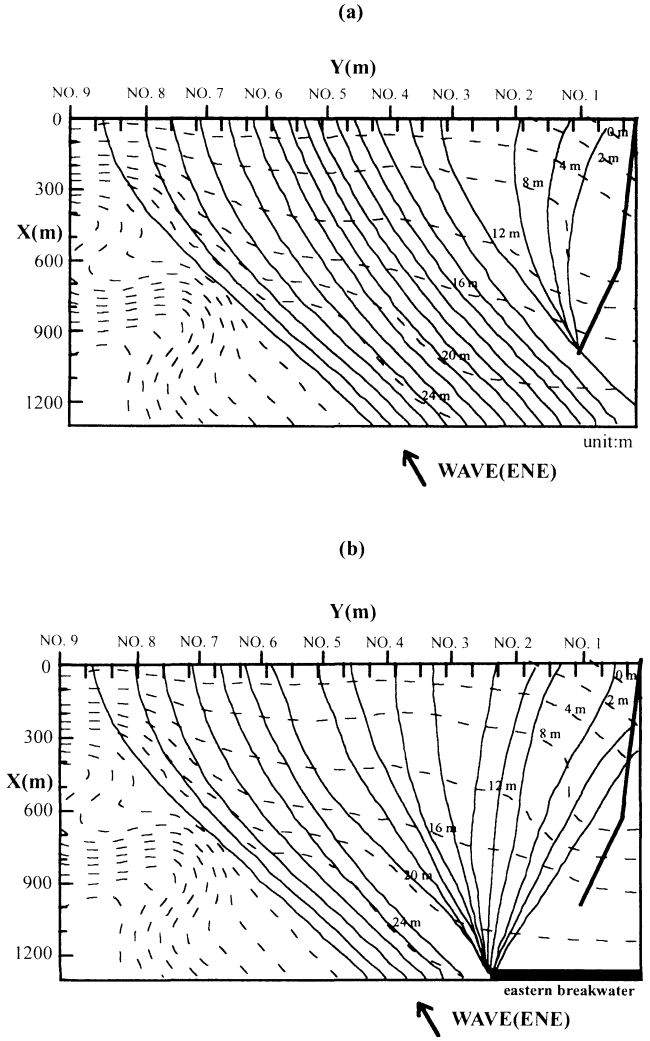

Figure 7. Wave rays at Hualien Coast for the monsoon wave condition; (a) without extended breakwater; (b) with extended breakwater.

CONCLUSIONS

Coastal topographical changes at Hualien Coast, Taiwan, are evaluated by using periodic field survey data and a statistical as well as a numerical model, which are previously successfully applied to respective topical studies. In the present study, the periodic field survey hydrographic data confirm the local reports of increased shoreline changes characterized by beach erosion in the southern zones and accretion in the northern zones of this coast after installation of an extended breakwater.

The measured beach profile data before the installation are then evaluated by a 2-D empirical eigenfunction model to generate statistical parameters for forecasting their variations in June, 1989 assuming no installation of an extended breakwater. The comparisons of the forecast values with the survey data along four typical beach profiles illustrate that their differences are more significant in the backshores of

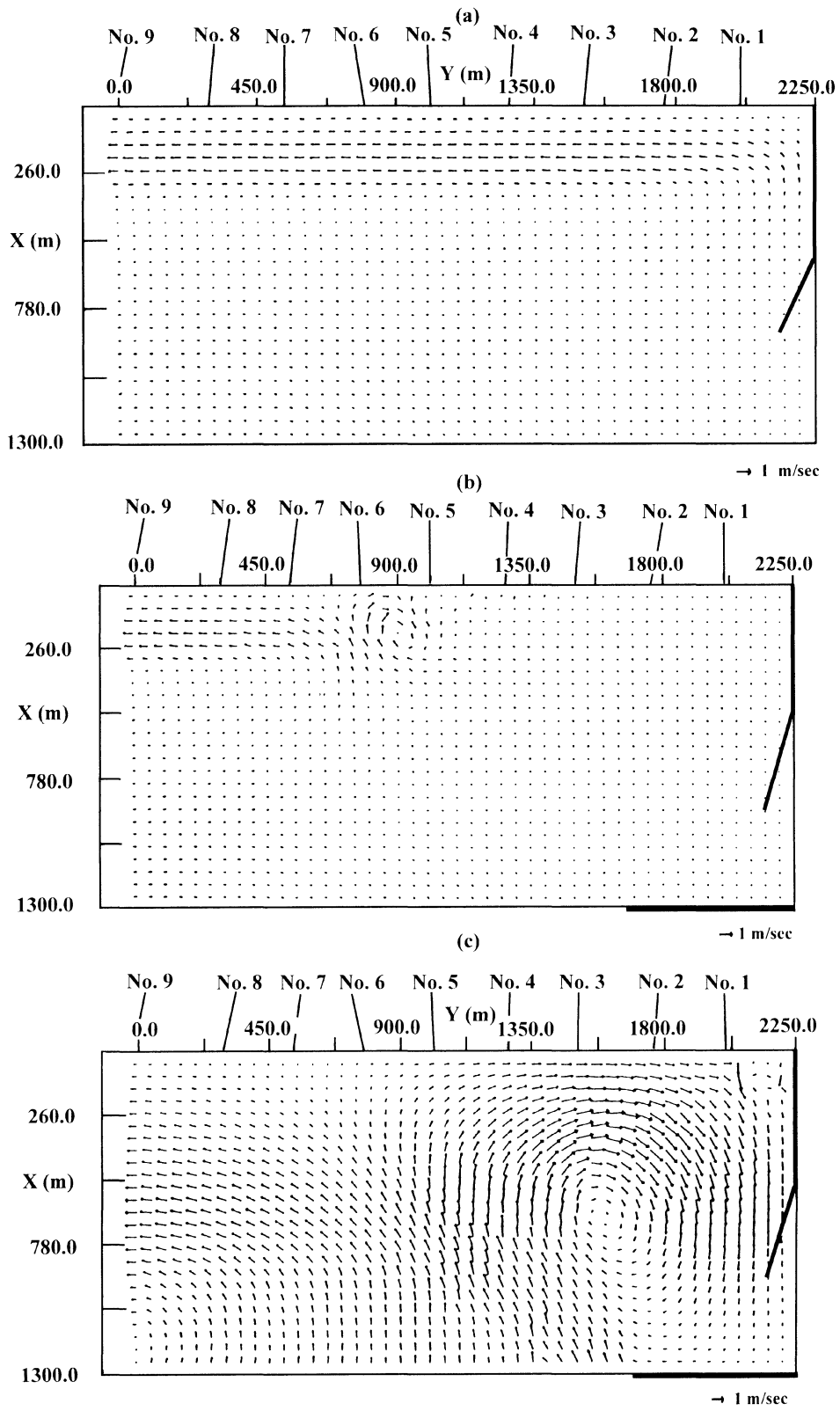

Figure 8. Nearshore current field at Hualien Coast before and after the extended breakwater due to (a): monsoon wave action without extended breakwater; (b): monsoon wave action with extended breakwater; (c): storm wave action with extended breakwater.

northern beach and foreshores of the southern beach. The results confirmed the tendency of shoreline changes along Hualien Coast and again suggest that the installation of the extended breakwater has caused substantial impacts.

Subsequently, a numerical model is employed to predict the nearshore hydrodynamics including wave and wave-induced current fields. The results clearly display that the extended breakwater could have reduced the wave heights at the harbor entrance by providing effective sheltering protection as it was designed for. However, it also results in a pair of circulation cell in the near shore water region and becomes greater during storm wave attacks. Thus, the causes of the shoreline changes are clearly identified by pointing out the formation of the circulation cell and the sediment transport associated with it. That is, the clockwise circulation of current transports the sediments towards the northern beach in the shallow water resulting in transports the sediments towards the northern beach in the shallow water resulting in increasing sediment accumulations near the outlet of Meilum River. The shortage of sediment supply causes an eroding southern beach for normal wave actions. Based on current evaluations by different schemes, the shoreline changes have been examined and the underlying mechanism are clearly identified. The results suggest that utilization of different reliable schemes with field survey data are very effective in evaluating the coastal topographical changes. In addition to the installation of the breakwater, the general reduction in sediment supply by the rivers due to flood control and unrestricted sand mining might cause beach erosion at Hualien Coast.

ACKNOWLEDGEMENTS

This study was supported partly by Agriculture Council and partly by National Science Council, Taiwan, under the grants of 82-AST-2.8-FOD-13(5) and NSC86-2611-E-006-019.

LITERATURE CITED

AUBREY, D.G., 1978. *Statistical and Dynamical Prediction of Changes of Natural Beach.* Ph. D. Dissertation, University of Calif., San Diego, California, 194p.

BERKHOFF, J.C.W., 1972. Computation of combined reflection-diffraction. *Proceedings 13th Conference on Coastal Engineering* (Canada, American Society of Civil Engineering), pp. 471–490.

BOOIJ, N., 1981. *Gravity Waves on Water with Non-Uniform Depth and Current.* Report No. 81-1, Department of Civil Engineering, Delft University of Technology, Delft, The Netherlands.

CHANG, C.K. and TZENG, H.M., 1993. Preliminary investigation for instability of Hualien harbor. *Proceedings 15th Conference on Ocean Engineering,* Taiwan, pp. 489–502. (in Chinese)

HORIKAWA, K., 1988. *Nearshore Dynamics and Coastal Process.* University of Tokyo Press, Japan, pp. 245–336.

HSU, T.W.; OU, S.H., and WANG, S.K., 1994. On the prediction of beach changes by a new 2-D empirical eigenfunction model. *Coastal Engineering,* 23, pp. 255–270.

HSU, T.W.; LIAW, S.R.; WANG, S.K., and OU, S.H., 1986. Two-dimensional empirical eigenfunction model for the analysis and prediction of beach profile changes. *Proceedings of 20th Conference on Coastal Engineering* (Taipei, ASCE), pp. 1180–1195.

HSU, T.W. and WEN C.C., 1998. *A Parabolic Equation to Inclined Water Waves and Wave Energy Transformation.* Report No. NSC86-2611-E-006-019, Department of Hydraulics and Ocean Engineering, National Cheng Kung University, Tainan, Taiwan.

ISOBE, M., 1987. A parabolic equation model for transformation of irregular waves due to refraction, diffraction and breaking. *Coastal Engineering in Japan,* 30, pp. 33–47.

LONGUET-HIGGINS, M.S., 1970. Longshore currents generated by obliquely incident sea waves, *Journal of Geophysical Research,* 75, 6778–6801.

NISHINURA, H., 1982. Numerical simulation of nearshore circulation. *Proceedings of 29th Conference on Coastal Engineering in Japan,* pp. 333–337. (in Japanese).

OU, S.H.; HSU, T.W.; CHANG H.K., and HAUNG Y.M., 1992. Wave and current fields at Nanbien Coast, Hualien. *Proceedings of 14th Conference on Ocean Engineering* (Hsinchu), pp. 107–127. (in Chinese).

PRUSZAK, Z., 1993. The analysis of beach profile changes using Dean's method and empirical orthogonal functions. *Coastal Engineering,* 19, pp. 245–261.

SONU, C.J..and JAMES, W.R. 1973. A Markov model for beach changes. *Journal of Geophysical Research,* 78(9), 1462–1471.

UDA, T. and HASHIMOTO, H., 1982. Description of beach changes using an empirical predictive model of beach profile changes. *Proceedings of 18th Conference on Coastal Engineering* (Cape Town, American Society of Civil Engineering), pp. 1405–1418.

WATER CONSERVANCY BUREAU, 1989. *Field Survey of Topographical Changes at Hualien Coast.* Engineering report, No. 76. 08002. 93-57 (2), Taiwan.

WINANT, C.D.; INMAN, D.L., and NORDSTROM, C.E., 1975. Description of monsoon beach changes using empirical eigenfunctions. *Journal Geophysical Research,* 1979–1986.